Can continuously recorded seismic data be improved with signal processing? The application of deconvolution to microseismic data

Ronald Weir, Laurence R. Lines, Don C. Lawton, and David Eaton

ABSTRACT

Passive seismic recording is increasingly being used to record seismic events associated with hydraulic fracture stimulation. The recorded amplitudes of these induced seismic events are relatively small and may be undetectable given the noisy environment in which they are recorded. Here we describe a method using reflection seismic processing techniques applied to continuously recorded passive (microseismic) data. Signal processing has been used for many years in reflection seismic processing to enhance signal quality. Algorithms such as deconvolution, scaling, and various types of filtering have been routinely applied to raw recorded data to enhance the processing and interpretability of the recorded data. Induced seismic events, such as perforation shots, can provide a time to depth relationship, although they may be difficult to detect. Induced seismic events caused by hydraulic fracturing events can indicate the depth and direction of the fracture stimulation, and induced seismicity may identify geohazards. In this study we apply a combination of the more commonly used algorithms used in reflection data processing to continuously recorded microseismic data and demonstrate how signal quality can be improved. These results demonstrate how signal processing can lead to more reliable detection of induced seismic events, and significantly improve the overall signal quality.

INTRODUCTION

Continuous seismic data (microseismic recording) is obtained by using very long seismic recording times, and capturing passive seismic events occurring at times during and after well treatments. These data are usually recorded in conjunction with well treatment programs, with seismic events occurring hours or days after hydraulic fracture stimulation. Several weeks of continuous data must be examined in order to identify seismic events. These events are identified, located in time, and attributes of the seismic events are determined. After an event is identified, calculations are made to determine the location (epicenter), depth (hypocenter), and type of event (strike-slip, normal, reverse, explosive), based on moment tensor inversion (Eaton, 2018).

The wave path for an induced seismic event is equivalent to one half of the two-way path for a reflection seismic event, originating from the same formation. For the reflection data, the seismic charge is located 15 meters below the surface, with the 3-C geophones located on the surface. The passive seismic array deployed had the 3-C geophones located 27 meters below the surface in shallow boreholes. In both cases the objective is to get information below the near surface low velocity layer; the buried seismic charge depth locates it below the low velocity, layer, the passive seismic array is also below the low velocity layer in shallow boreholes.

There may be variations in the coupling of the geophone causing variances in the recorded amplitude on a trace to trace basis. This variance requires a trace by trace

amplitude equalization to compensate for geophone variance. Noise considerations for both reflection seismic data and passive data recording are similar. There is 60 cycle interference from overhead power lines, noise from producing wells, pipelines, vehicle traffic, and drilling activities. In both cases the objective is to improve the signal to noise ratio within the usable bandwidth of the seismic data.

Seismic event picking changes significantly using deconvolved data, in that the seismic event is located on a maximum peak or trough amplitude. Usually seismic event picks are selected at the onset of the seismic event De Meersman et al. (2009), these data have had their source frequency spectrum shifted to the zero-phase equivalent (Margrave 2005) by means of a zero-phase deconvolution. Techniques such as short term and long-term averaging (STA, LTA) may have to be modified, due to the change in the dominant frequency of the recorded data as a result of the deconvolution.

THEORY

A passive seismic event, whether an earthquake (magnitude 4 or greater) or an event resulting from hydraulic fracturing (magnitude <4) share certain characteristics, a P wave followed by an S wave. With large earthquakes, there may also be the later arrival of surface Love waves and Raleigh waves. These events are generally identified with the first arrival, generally a positive or negative deflection observed in the geophone. Seismic reflection recording will also generate Raleigh waves, seen on the seismic record as "ground roll."

A seismic reflection section records both direct and reflected arrivals. The first arrivals, called first breaks, arrive as an onset either with a positive or negative deflection in the geophone. The recorded data also contains the reflection information, multiples, and coherent and random noise. The amplitude spectra of the raw seismic record are typically skewed to the lower frequencies. The dispersive nature of the earth may cause the higher frequencies to travel faster than the lower frequencies, creating a discrepancy between the phase velocity and the group velocities.

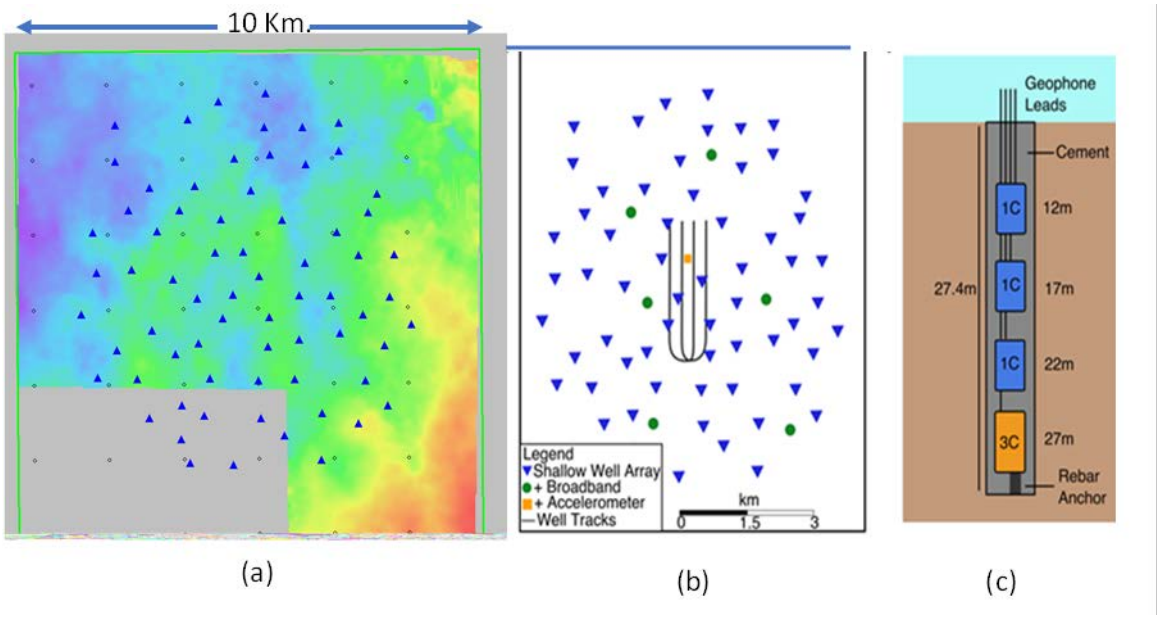

FIG. 1. Location of the passive recording array, and the subsurface configuration. Most of the TOC2ME passive recording stations are co-located with the 3-D, 3-C seismic program. (a) is the TOC2ME buried geophone array plotted over a time structure map of the Swan Hills Formation, (b) shows the TOC2ME array plotted with the treatment wells, and (c) is the layout of the buried 3-C geophone array.

Recognizing the fact that the recorded data is band limited, the challenge becomes to identify the usable frequencies where the signal resides. In reflection seismology, the processing objective is to have the data represent the "true" reflectivity convolved with the zero-phase wavelet, given the input is generally a mixed phase wavelet (Margrave 2005). The objective for processing passive seismic data is similar and involves converting the mixed wave source generated by the subsurface seismic event to a spike and balancing the frequency spectrum to that generated by the source.

As a cautionary note, the data generated by the spiking deconvolution process is not suitable for "Brune" type of analysis (Walter and Brune, 1993), where seismic event properties are determined by a low-frequency plateau and a corner frequency. Spiking deconvolution whitens the frequency spectrum and creates a more or less constant roll off in the high frequency content of the entire data set.

Deconvolution overview

Higher frequencies within the usable bandwidth can be recovered in reflection data using deconvolution, which deconstructs the data into its discrete frequency components, and balances the amplitudes of the constituent frequencies in the data by boosting the high frequencies. In balancing the frequency spectra, deconvolution also brings up the high frequency noise contained in the data (flattening the frequency spectra). The data is subsequently filtered to recoverable signal (based on examination of the frequency plots), and the filtered data is output. A second pass of deconvolution, called a zero-phase operator, is applied to shift all usable frequencies to zero phase. This creates the zero-phase equivalent of the source wavelet and compensates for high frequency attenuation.

The net result of this is that the seismic event now has an event corresponding to a maximum peak, or trough depending on the nature of the source. The result of this process is shown as applied to several continuous seismic records and are displayed in the three examples in this paper.

Deconvolution is universally applied to most reflection seismic data (Leinbach 1991). Here we will discuss the application of deconvolution to passive seismic data. In reflection seismology a source waveform is generated from either impact, dynamite, or a Vibroseis source. In general terms, the source wavelet penetrates the earth and is reflected to back to the surface to be recorded at surface geophones. In Vibroseis recording, the long source wavelet is converted to a Klauder wavelet (zero phase) by autocorrelating the sweep with itself (Margrave 2006). Dynamite data, as recorded, is generally mixed phase. For picking seismic events in reflection data, the ideal wavelet (after processing) is zero phase, aligning the maximum energy (peak or trough) with a seismic reflector. Here, we will treat the passive seismic event as a deep seated seismic source, the one-way equivalent of a single reflected seismic event.

For a zero-incident vertical wave, the amount of energy reflected at each geological interface is governed by the following equation:

$$\boldsymbol{Rn} = \frac{\boldsymbol{\rho_n v_n - \rho_{2n+1} v_{n+1}}}{\boldsymbol{\rho_n v_n + \rho_{n+1} v_{n+1}}} \quad (1)$$

where ρnvn is the density and sonic velocity of the nth layer respectively. This equation also applies to zero incidence shear waves; however, shear wave sources are relatively uncommon in reflection seismology. A wavelet generated by a dynamite source is generally mixed phase, as are impact sources (Robinson, 1980). With Vibroseis®, the source is known, with both types of sources the earth will attenuate the higher frequencies, and the phase may shift over different frequencies on the returned signal. Shear wave sources are not commonly used in reflection seismic data acquisition as a source; however, shear waves are often recorded as converted waves (Figure 2).

The convolutional model for seismic reflectivity can be expressed as:

$$T_{pp}(t) = W_p(t) * R_p(t) * I(t) + N(t) \text{ for P-P reflections} \quad (2)$$

$$T_{ps}(t) = W_{ps}(t) * R_{ps}(t) * I(t) + N(t) \text{ for P-S (converted) reflections} \quad (3)$$

where R(t) is the reflectivity series, W(t) is the source wavelet, I(t) is the instrument response, and N(t) is noise, all as a function of time, and * is the convolution operator. In this situation, T(0) is known, as the origin of the seismic source.

In this case, the reflection coefficient series, Rp(t), can be considered a component of the more general Green's function.

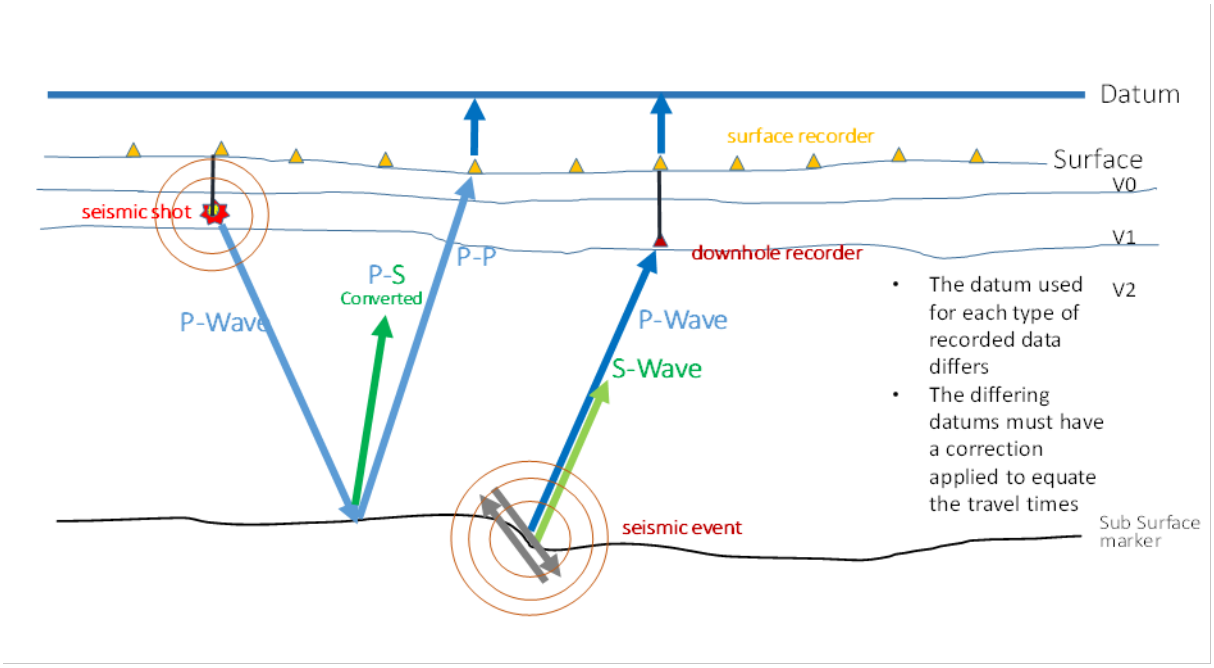

FIG. 2. An illustration of the passive and active seismic sources. The passive seismic event can be thought of as the one-way equivalent of a reflected seismic event coming from the same depth. Attenuation effects will be similar in that the seismic signal travels through the same media on its way to the geophone recording array.

For continuous seismic data, T(0) is not known, and the recorded signal is a direct arrival.

$$T_p(t) = W_p(t) * G(t) * I(t) + N(t) \text{ for P arrivals} \quad (4)$$

$$T_s(t) = W_s(t) * G(t) * I(t) + N(t) \text{ for S arrivals} \quad (5)$$

where Tp(t)is the p wave time direct arrival, Ts(t) is the direct shear wave arrival, and N(t) is noise, all as a function of time. G(t) is a Green's function describing the subsurface impedance, and I(t) is the instrument response.

In this situation, T (0) is unknown, the origin of the seismic source. Induced seismic events such as strike-slip movements may be the result of a double couple event, producing significant shear waves as a primary source. Explosive events such as perforation shows may only generate P waves. For reflection data, T(0) is known, either with the detonation of a dynamite charge, or the onset of a Vibroseis sweep. T(0) is not known for subsurface natural or induced seismic events.

In a seismic reflection survey, the objective of deconvolution, is to balance the spectrum where signal exists, reduce the nose, and display the final data as a least squares approximation of a spike (delta function). This ensures that a seismic reflector (an event) is on a peak or a trough, which correspond to a positive or negative reflection coefficient. This enables the data to be tied to well log data by means of a synthetic seismogram, and the time picks can accurately be converted to a depth map for structural interpretation. The seismic event is centered on a strong peak or a trough, and because the event is not a spike, has associated side lobes. The onset of the seismic reflecting event after deconvolution is

applied occurs in negative time, a few milliseconds in advance of the main event (Figure 3.).

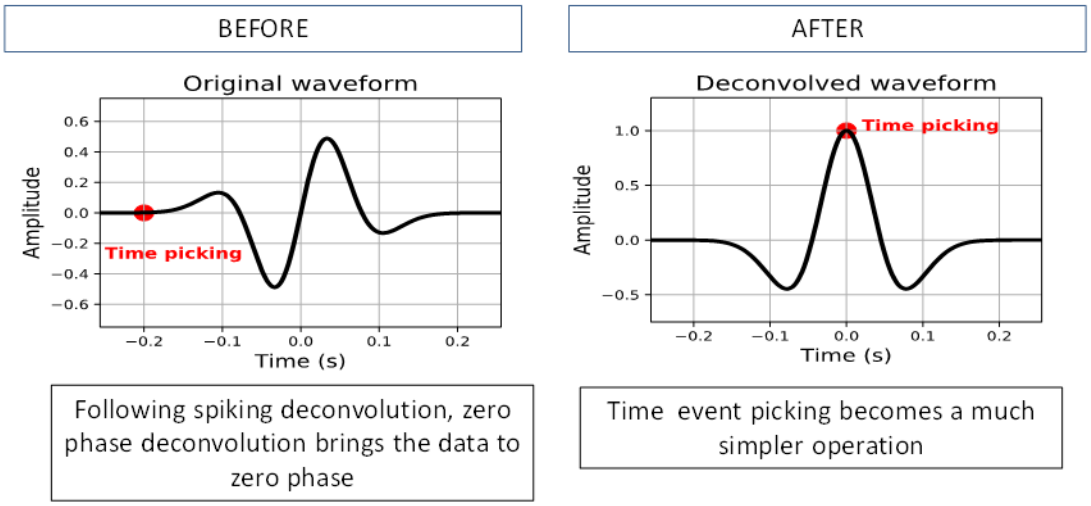

FIG. 3. A schematic diagram of the effect of zero phase deconvolution, and how seismic events are picked. The onset of a seismic event on raw data is correlated as the seismic event; the deconvolution processed data shifts the phase spectrum to zero phase, such that the event is picked on the maximum amplitude. Note the location of the seismic picks, denoted by the red circles, before and after processing.

For passive microseismic seismic events, induced seismicity, and earthquakes, the onset of the event is the initial deflection of the geophone as the P and S waves arrive from the event. Appling the aforementioned process to passive seismic data will have the same effect; the event will be correlated as a peak or trough, depending on the position relative to the source, and whether it is a double couple or explosive source. Seismic event picking becomes a matter of identifying a maximum peak or trough, and correlating it with nearby stations, in contrast to identifying the initial onset of the seismic coda (Eaton 2018).

METHOD

In order to process continuous recorded data, the seismic data is segmented into 60 second time intervals (the SEGY limit). With the data formatted in this fashion, the recorded data segments are loaded into commercial processing software. Each record contains vertical, (Z) and lateral (H1 and H2) components of recorded data, from the TOC2ME buried geophone array. The Z channel captures the P wave arrival (vertical component), the H1 and H2 channels capture the two orthogonal horizontal components of the S wave arrival.

Seismic records known to contain perforation shots and induced seismic events resulting from fracture stimulation were processed to determine the effectiveness of deconvolution on improving data quality. Side by side comparisons of raw to processed data are displayed in the three examples shown in this paper to demonstrate the effect of filtering and deconvolution.

Parameters that are user defined are operator length, design gate and pre-whitening. The operator length was 80 ms., like that used for reflection data. Pre-whitening is a stability factor that is introduced given that there are frequencies where the spectrum of the estimated wavelet is small (Margrave 2005). Here we applied a 1 % (or 0.01), pre-whitening factor. The design gate is a window that contains seismic events.

The bandpass filter was chosen on the basis of examination of the spectral output of the deconvolved trace. Here we applied a 75 Hz. High cut, again consistent with results obtained from the overlying reflection PP-PS survey. As a final step, the data was converted to minimum phase, within the estimated bandwidth of the recorded data, as close as we can get to a "spike" representing the band limited equivalent of the delta function.

A reflection seismic record may contain 20 or more identifiable events in the space of a 3 second record; whereas, there are comparatively few, if any, recorded events on a continuous 60 second record. In reflection data, the operator design is typically centered over known reflectors. For the continuous data the operator was applied to the entire trace as a first pass. Once events such as perforation shots and hydraulic fractures are identified, the operator is redesigned using a 1000 ms. window centered on an identified passive seismic event.

RESULTS AND ANALYSIS

Figure 4 shows a P-P seismic reflection section through the treatment area, plotted alongside a spectral plot. These reflection data were generated from a dynamite source and recorded for both PP and PS components. The maximum frequency obtained at the target from reflection seismic data was approximately 65 Hz. The arrow indicates the Duvernay formation treatment interval, the target depth at which induced seismicity is expected. The seismic signal produced by the induced seismic event, and the P-P reflection seismic data travel through the same geological section, albeit one way for the induced event, and two way for the seismic reflection event. The spectral analysis in both data sets has a maximum frequency of around 65 Hz.

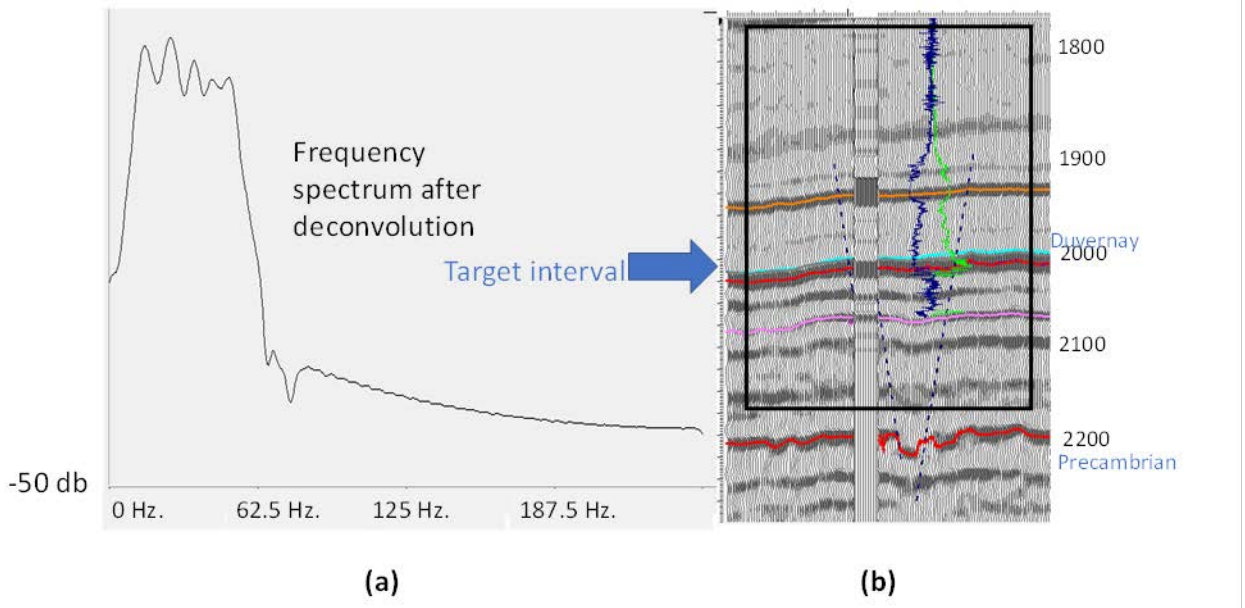

FIG. 4. A cross section of seismic reflection data showing the spectrum of the seismic data (a), calculated from the interval shown in the box in (b). The treatment time/depth on seismic reflection data, as well as a log showing the deep well tie is shown in (b). MicroSeismic events are expected to originate in or near the treatment time / depth interval as shown with the arrow. The P-P reflection data has a maximum frequency of around 65 Hz. The arrow highlights the target zone for hydraulic fracturing, the induced seismic events are expected to originate in or around this zone.

All the continuously recorded 60 second records in this study were processed by loading the SEG 2 or SEG D data into the processing system. An initial pass of a Werner (Spiking deconvolution was applied to the entire record, using an 80 ms. operator and a 1 % pre-whitening stability factor (this is very similar to the first processing quality control step used in land processed reflection data).

An Ormsby filter was applied using a bandpass of 8-12-60-70, as this was the estimated usable frequency in the data. The traces were balanced using a total trace average. Some of the traces had very high overall amplitudes due to noise trains. The trace balancing brought the amplitude of these traces to be in line with the rest of the data. This in turn made the recorded seismic data easier to interpret.

The zero-phase operator was applied to condition the data as shown in Figure 3. All frequencies within the usable bandwidth were shifted to zero phase, and the data was displayed. Seismic events were qualitatively identified, and the initial deconvolution used in the first step was redesigned using a 1000 ms. window over an identified event, and the process was repeated using data designed over an identified seismic event. These data were displayed, and output to SEGY format for analysis.

There are three examples of continuous data used here. The first example is a perforation shot in a low signal to noise environment. The second example is an induced

event with P and S arrivals. The third example in this study was passed on to an auto picking event detection process (kurtosis) and the results displayed on the seismic data.

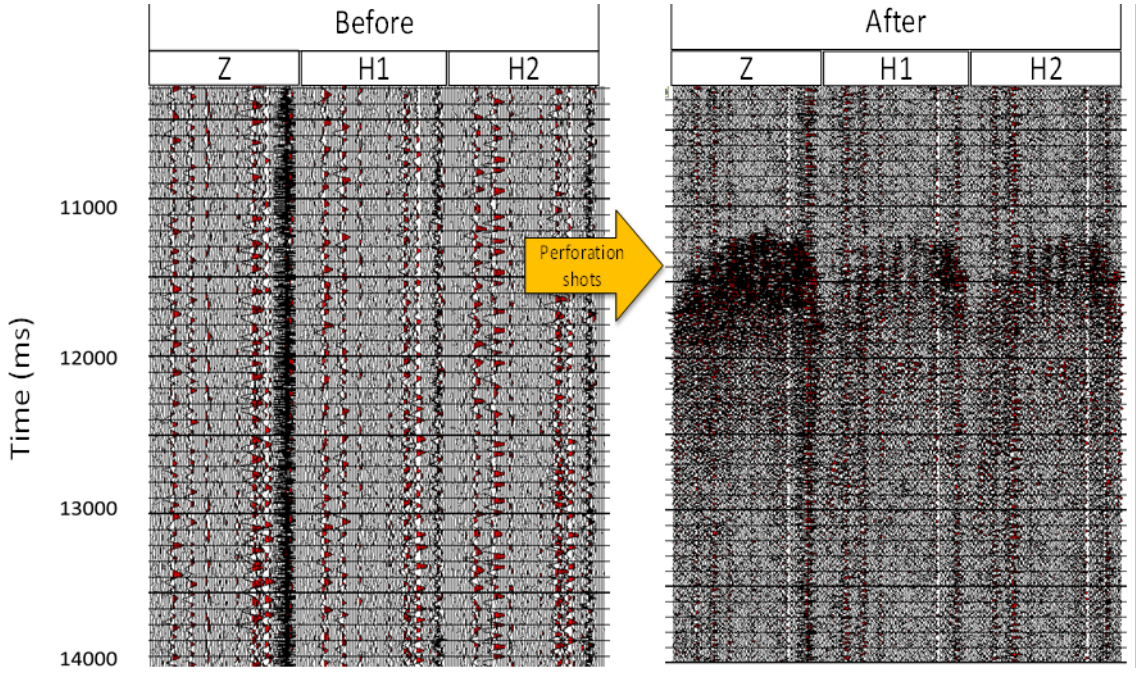

FIG. 5. A continuous seismic record shown before and after processing. The data shown is the vertical components, Z, H1 and H2 components. Seismic events are difficult to identify on the raw data (a) are visible at the 11300 ms. highlighted with the arrow.

Example 1, perforation shot

Figure 5 shows a spectral display of a 4 second portion of a continuous seismic record containing induced seismic events before and after deconvolution. For this seismic record, the 2nd pass of deconvolution was centered on 11500 ms. Using a 2000 ms. design gate. There is an increase in the frequency of the processed record and the anomalously strong traces on the raw record have been scaled to match the rest of the data.

Figure 6 is a spectral display of the same two records from Figure 5. The deconvolution processing has flattened the frequency spectrum, bringing the frequencies up to 65 Hz, and beyond. Frequencies above 65 Hz. were interpreted to be noise and were filtered out using an Ormsby bandpass filter.

The result shown here for the perforation shot demonstrates a significant improvement in the seismic signal to noise ratio. A seismic event has become visible, notably on the Z channels, and to a lesser extent on the H1 and H2 channels. These events are not obvious on the unprocessed data in, but are quite visible as highlighted by the yellow arrow in Figure 5. This processing flow shows promise in the identification of events such as perforation shots, which have in many instances, been difficult to pick.

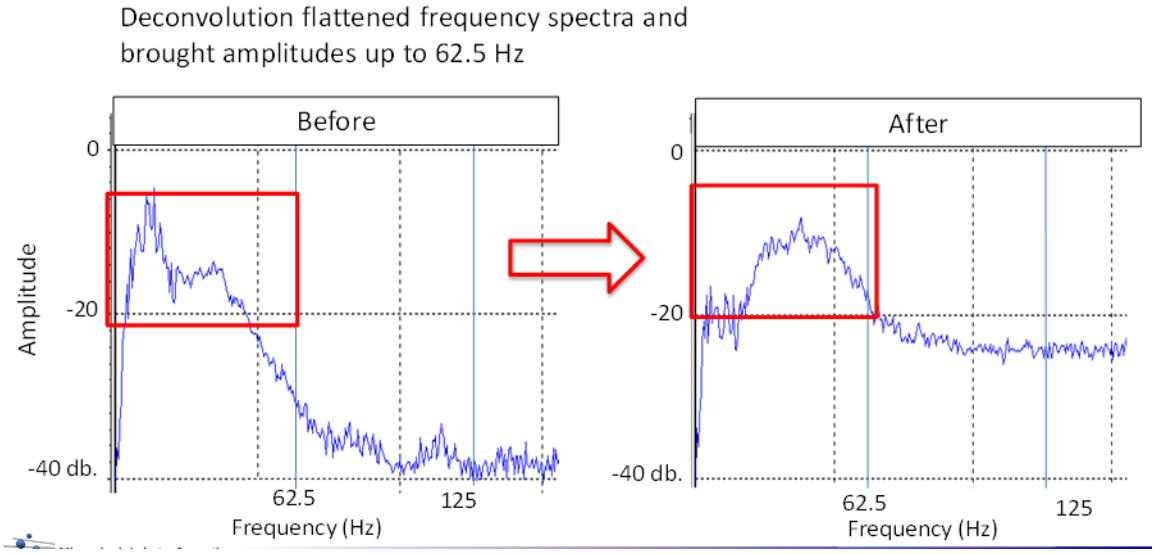

FIG. 6. A spectral analysis of the 60 second record from Figure 5, before (a) and (b) after deconvolution. The effect of the spiking (Weiner) deconvolution is to balance the frequency spectra. The recovered frequency spectrum of the continuous data decreases significantly to 65 Hz.

Example 2, induced seismic event

A 2nd example of pre and post deconvolution is shown in Figure 7. In this example, the seismic records are sorted in terms of offset distance with respect to the calculated hypocenter. The seismic event shows NMO (normal move out) on both the raw and processed data. The effect of the processing is to sharpen up the event and balance the amplitudes in the traces. There is a significant improvement in the P wave arrivals, the S wave arrivals appear to be somewhat degraded although still visible.

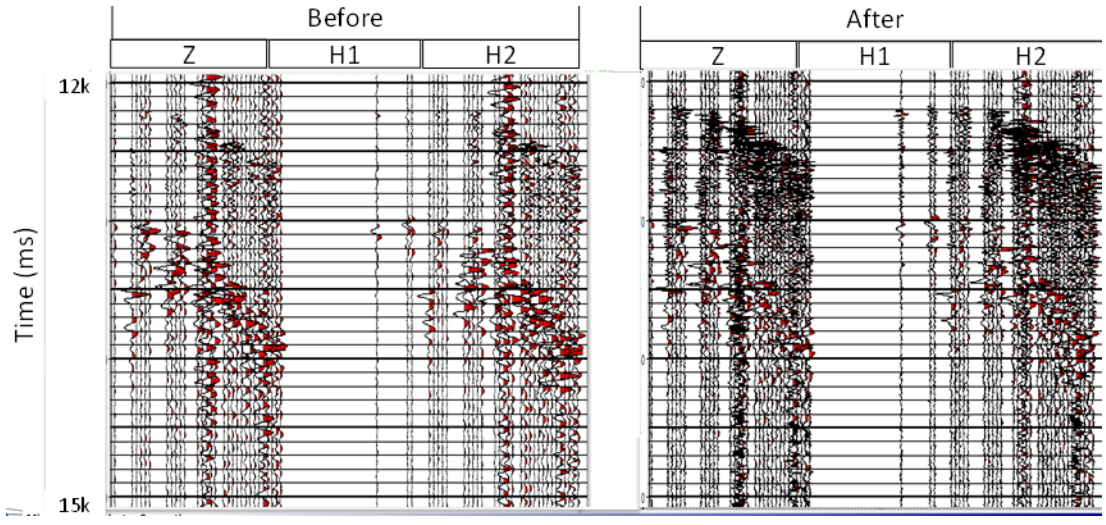

FIG. 7. Seismic records sorted in offset distance with respect to a seismic event before and after deconvolution. There is a noticeable improvement in the P arrival (12500 ms.), there is no obvious improvement in the S arrival, although the signal is apparent (13000 ms.).

Example 3, auto picking

For the third example, a seismic record with an event of low signal-to-noise ratio (SNR) is processed and analyzed using auto picking on data before and after deconvolution. The data is composed by vertical and two horizontal channels containing P and S-waves. The intent of this example is to present a workflow to retrieve arrival-time picking (ATP) information using deconvolved passive seismic data in situations where the recorded data has a low signal to noise ratio. A comparison is presented applying an ATP workflow to pre and post processed data. In this situation conventional methods may generate ambiguous results. For a complete discussion on the ATP picking algorithm used here, I refer the reader to Paes and Eaton (2018). In these examples, ATP picking was used on the raw data. On the deconvolved data, ATP picking was used the maximum amplitude.

To use the kurtosis auto picking method, an existing catalog containing known seismic events are used. These events were based on the corresponding clock time of reservoir stimulation and perforation events. The events used in this example were extracted from a catalog generated by the energy-stack algorithm (Paes, 2018). Recorded seismic data matching the time of the perforation and stimulation events were loaded, filtered, and auto picked to identify seismic events.

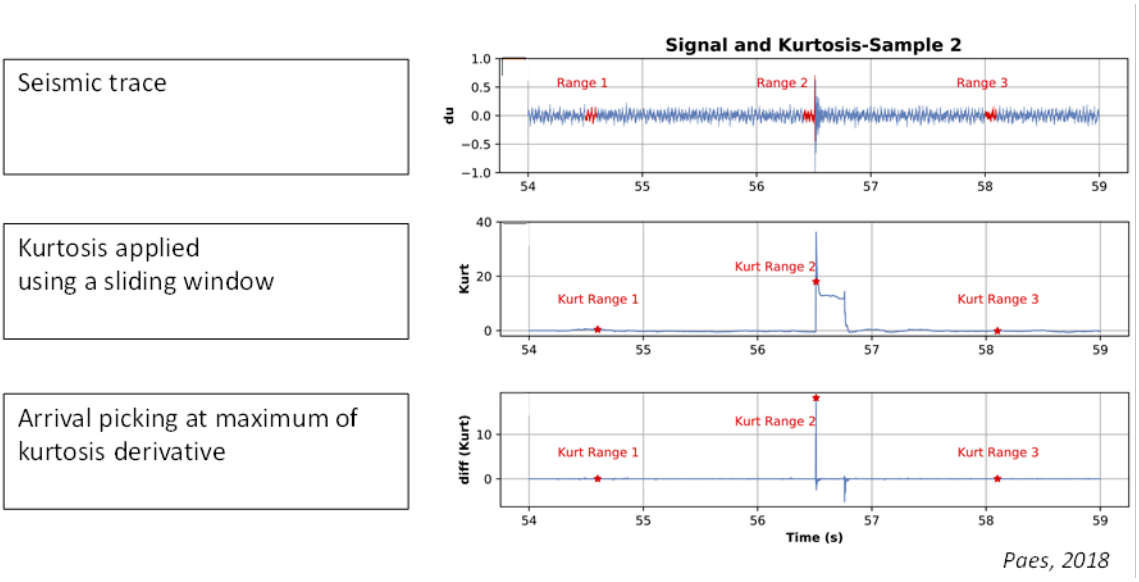

FIG. 8. The kurtosis picking algorithm uses a time ranges derived from known seismic events (pilot trace) and uses them to detect events on the continuous record (Pays, 2018). This method is used in the examples in Figures 9 and 10 to detect P and S arrivals.

The first method (before data deconvolution) for ATP uses the kurtosis derivative (differential kurtosis) as the characteristic function (CF) (Paes, 2018). A step-by-step of the CF building and ATP) using differential kurtosis algorithm is shown in Figure 8. The trace shown is used as CF on the picking algorithm. Information from the seismic picks on neighboring events is also used to aid in the identification of seismic arrivals. The differential kurtosis algorithm was applied on the low SNR event. Figures 9 and 10 display the raw data with the ATP event picks in red.

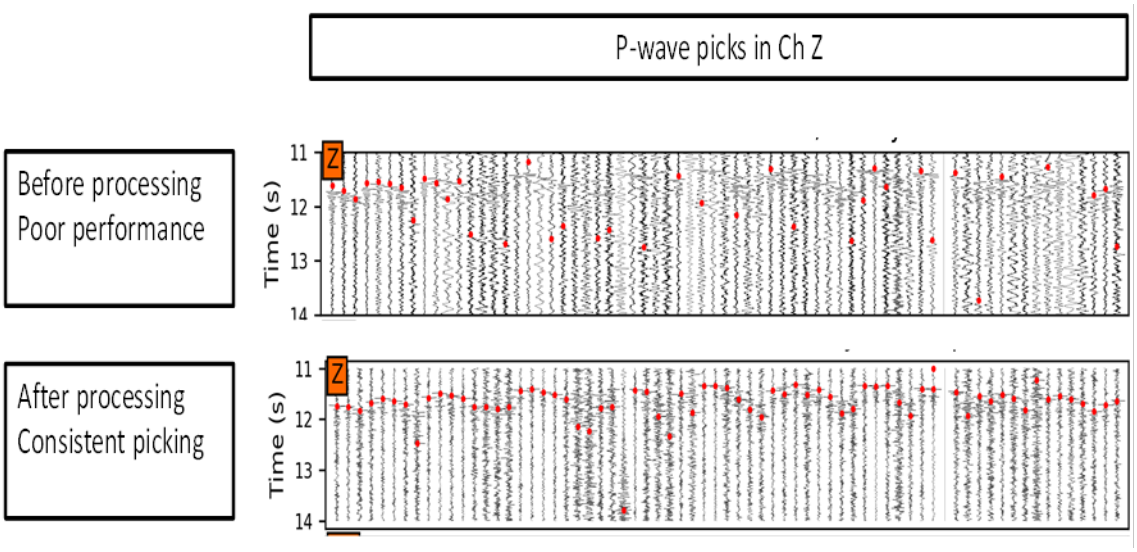

FIG. 9. An example of a raw seismic record showing arrival picks using differential kurtosis algorithm (ATP) upper, and the deconvolved record (lower). There is a significant improvement in the picking of the P wave arrivals in the deconvolved data.

The second method used for ATP processing is applied on traces after deconvolution. Figures 9 and 10 show the result of basic trace-maximum identification (the first step of an ATP algorithm). The conversion of the wavelet to zero phase, and the signal to noise improvement have made identification of microseismic events easier and the (previously complex) algorithm for ATP simply becomes the identification of maximum peak or trough into a limited time window.

In Figure 9, the early maximum peak of each z-channel was limited to a restricted time window around 12 seconds and used as the P-wave onset. These ATP picks are shown as red dots in the figure. Figure 9 shows the comparison of the seismic event picking on the vertical (z) channels for the pre and post deconvolved data. The number and quality of the P event arrivals show significant improvements for the P arrivals on the deconvolved data.

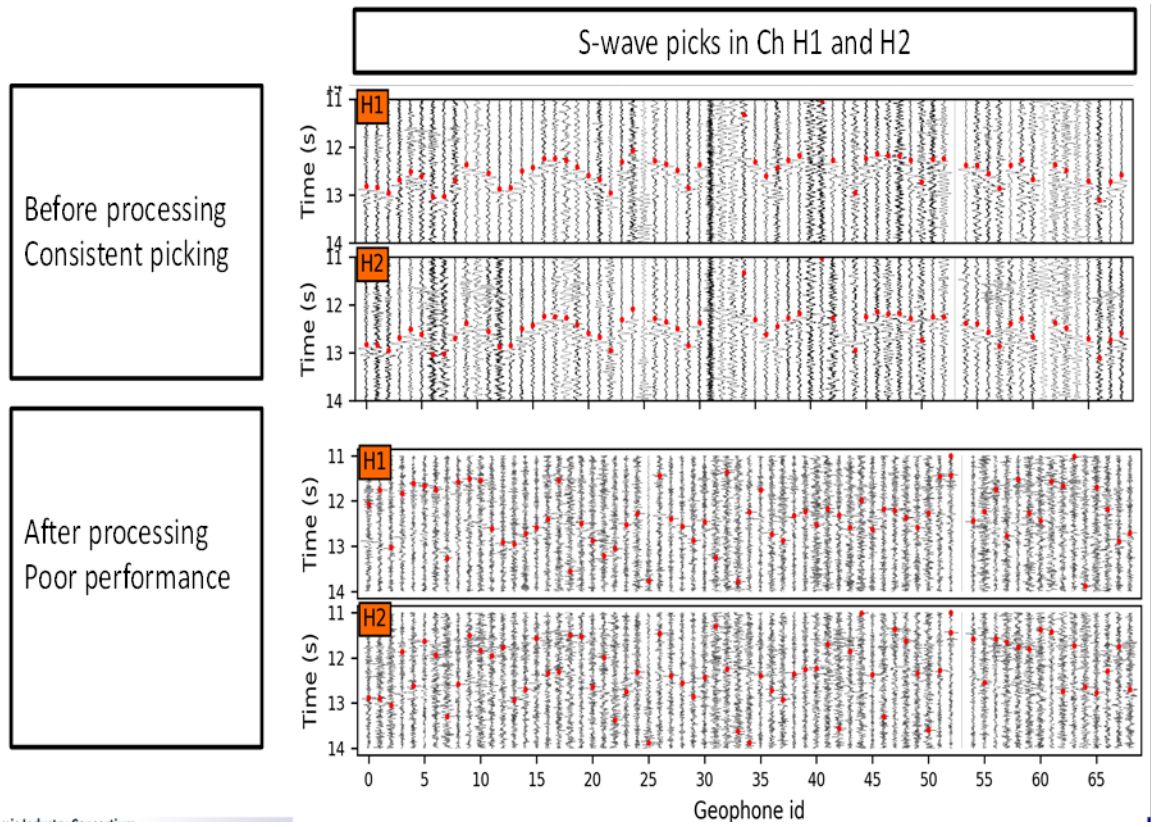

FIG. 10. An example of the same record shown in Figure 9, after processing, this time displaying the H1 and H2 components. The processed records have been picked for events using ATP maximum seismic amplitude. The top panel was picked using kurtosis. The S arrivals appear to be more consistent on the raw data, the processing flow seems to have degraded the S arrivals.

The S-wave is picking (Figure 10.) is dependent on the P wave pick and is limited to a maximum time window from 0.5 to 2.5 seconds below the P arrival (as identified on the z-channel). The automatic picking for shear events on the H1 and H2 channels may identify spurious events or outliers, so a comparison of events on the H1 and H2 channels is used as a quality control step for these events. If there is a large difference (H1 and H2, > 0.5 s), the calculated S arrival-time is set to be the one with ATP closest to the S-arrival of the seen on the neighboring geophones.

Figure 10 shows the result for the S wave picking for both the pre and post deconvolved data. The horizontal H1 and H2 channels are shown, with the corresponding picks in red. The post processing shows some of the same picking results as the original data, but with considerably more scatter. The picks on the original data. It appears that the deconvolved data using this processing flow is less suitable for S arrivals.

The picks for the P waves appear to be more consistent for the deconvolved data (Figure 10) than for the raw data. The reverse is true for the S arrivals as shown in Figure 10. They are more consistent across the Z time window. The shear wave response is less consistent, although the picking algorithm may need to be optimized for deconvolved S wave events.

CONCLUSIONS

Given the examples shown here, reflection seismic data processing has useful applications in the conditioning of continuously recorded seismic data for microseismic monitoring. Processes such as deconvolution, filtering and scaling can enhance the signal to noise ratio and improve the ability of auto picking algorithms to detect events. The results obtained from the P wave arrivals show considerable promise in identifying P wave arrivals, particularly in noisy data.

The processing used here may not be suitable for S arrivals. It is possible that most of the S wave energy resides in the lower frequency band (around (10 Hz. Or lower). The results here suggest a best practice may be to use a dual stream method, separate processing flows for the P and S arrivals. The S wave arrivals are more identifiable in the unprocessed data, so it may be prudent to eliminate the spectral balancing.

With the examples we have shown here, conventional seismic processing can add valuable information to microseismic event detection and interpretation. Techniques applied to reflection seismic processing can be readily applied to continuous seismic recording and yield similar results. This technique can bring out and help identify seismic events that were previously undetectable as well as retrieving ATP from the large number of events with so low SNR that conventional methods are unable to process.

FUTURE WORK

A process specifically designed to enhance S arrivals will be developed. The downhole geophones used to record this data were 10 Hz, so instrument and geophone complementation could be applied to recover some of the low frequencies.

Zero phase deconvolution without the spectral balancing may be more suitable for the S wave response. Additional trace to trace techniques such as surface consistent deconvolution, FX and FK filtering may also be applied. For this study, only single trace operations were applied. Deconvolution operators specific to S and P wave events can also be designed, to further enhance detectability, particularly on low signal to noise data, and weaker seismic events.

A specific work flow will be designed to enhance the shear wave seismic data. The lower dominant frequency inherent in the shear wave data lends itself to this type of processing, possibly using modified design gates and operator lengths.

ACKNOWLEDGEMENTS

We are grateful to TGS Seismic Solutions for providing the 3D multicomponent data, Schlumberger for providing the VISTA software used in this study and. We thank the sponsors of CREWES for their financial support of this study. This work was also funded by NSERC (Natural Science and Engineering Research Council of Canada) through grants CRDPJ 461179-13, CRDPJ 474748-14, IRCPJ/485692-2014, and IRCSA 485691. We thank Andrew Poulin, Thomas Eyre, Atila Paesastaff, and students at the University of Calgary for technical assistance. We are grateful to CGG for providing Hampsen-Russell software used in this study, and Seisware for the use of their interpretaion software. We

thank Divestco for providing digital LAS curves. We also thank The SEG Earl D. & Reba C. Griffin Memorial Scholarship.

REFERENCES

De Meersman, K., M. Van der Baan, J.M. Kendall, (2006) Signal extraction and automated polarization analysis of multicomponent array data. Bulletin of the Seismological Society of America, 96(6), 2415-2430.

Eaton, D. (2018) Passive seismic monitoring of induced seismicity, Fundamental Principles and Application to Energy Technologies. Cambridge University Press.

Einspigel, David and Leo Eisner (2013). The differences in the detectability of perforation shoats and microseismic events in the surface monitoring. The attenuation effect. Acta Geodyn. Geomater., Vol. 11, No. 2 (174), 159–164, 2014

Paes, Atila and David W. Eaton (2018) Energy-stack and Kurtosis: the dynamicduo for microseismic event identification, Microseismic Industry Consortium Annual research report, Vol. 9, 2018

Robinson, Enders A., Sven Treitel. (1980) Geophysical signal analysis, Prentice-Hall Inc, Englewood Cliffs, N.J.

Leinbach, Jim (1995). Wiener spiking deconvolution and minimum-phase wavelets: A tutorial. The Leading Edge, 14(3), 189-192. fore and after.

Margrave, G. F., (2005). Methods of seismic Data Processing Geophysics 557/657 Course Lecture Notes. The CREWES project, Department of Geology and Geophysics, The University of Calgary.

Walter, W.R. and J.N. Brune 1993.Spectra of seismic radiation form a tensile crack. Journal of Geophysical Research: solid earth, 98(4), 1110-1118